Unveiling Unprecedented Methane Hotspots in China's Leading Coal Production Hub: A Satellite Mapping Revelation

Ge Han, Zhipeng Pei, Tianqi Shi, Huiqin Mao, Siwei Li, Feiyue Mao, Xin Ma, Xingying Zhang, Wei Gong

AGU ADVANCING EARTH AND SPACE SCIENCES

Geophysical Research Letters

RESEARCH LETTER
10.1029/2024GL109065

Unveiling Unprecedented Methane Hotspots in China's Leading Coal Production Hub: A Satellite Mapping Revelation

Ge Han[1,2], Zhipeng Pei[3], Tianqi Shi[4], Huiqin Mao[5], Siwei Li[1], Feiyue Mao[1], Xin Ma[3], Xingying Zhang[6], and Wei Gong[3,7,8]

[1]Hubei Key Laboratory of Quantitative Remote Sensing of Land and Atmosphere, School of Remote Sensing and Information Engineering, Wuhan University, Wuhan, China, [2]Perception and Effectiveness Assessment for Carbon-neutrality Efforts, Engineering Research Center of Ministry of Education, Institute for Carbon Neutrality, Wuhan University, Wuhan, China, [3]State Key Laboratory of Information Engineering in Surveying, Mapping and Remote Sensing, Wuhan University, Wuhan, China, [4]Laboratoire des Sciences du Climat et de l'Environnement, Université Paris-Saclay, Gif-sur-Yvette, France, [5]Ministry of Ecology and Environment Center for Satellite Application on Ecology and Environment/State Environmental Protection Key Laboratory of Satellite Remote Sensing, Beijing, China, [6]Key Laboratory of Radiometric Calibration and Validation for Environmental Satellites, National Satellite Meteorological Center, China Meteorological Administration, Beijing, China, [7]Electronic Information School, Wuhan University, Wuhan, China, [8]Wuhan Institute of Quantum Technology, Wuhan, China

Key Points:

- Satellite data identify 82 major methane emitters in Shanxi, China, with high annual emissions of up to 1.2 Mt
- Top 20% of coal mines contribute to half of the region's total methane emissions
- Findings highlight the importance of direct measurements for accurate emission estimates

Supporting Information:

Supporting Information may be found in the online version of this article.

Correspondence to:

Z. Pei,
peisipand@whu.edu.cn

Citation:

Han, G., Pei, Z., Shi, T., Mao, H., Li, S., Mao, F., et al. (2024). Unveiling unprecedented methane hotspots in China's leading coal production hub: A satellite mapping revelation. *Geophysical Research Letters*, *51*, e2024GL109065. https://doi.org/10.1029/2024GL109065

Received 4 MAR 2024
Accepted 13 MAY 2024

Author Contributions:

Conceptualization: Ge Han, Zhipeng Pei
Funding acquisition: Ge Han
Investigation: Zhipeng Pei, Tianqi Shi
Methodology: Zhipeng Pei
Resources: Tianqi Shi, Huiqin Mao, Xingying Zhang
Software: Zhipeng Pei
Supervision: Ge Han, Huiqin Mao, Siwei Li, Feiyue Mao, Xin Ma, Xingying Zhang
Validation: Zhipeng Pei
Visualization: Zhipeng Pei
Writing – original draft: Zhipeng Pei
Writing – review & editing: Ge Han

Abstract China is likely the world's largest anthropogenic source of methane emissions, with coal mine methane (CMM) being the predominant contributor. Here, we deploy 2 years of satellite observations to survey facility-level CMM emitters in Shanxi, the most prolific coal mining province in China. A total of 138 detected episodic events at 82 facilities are estimated to emit 1.20 (+0.24/−0.20, 95% CI) million tons of methane per year (Mt CH_4/yr) during 2021–2023, roughly equivalent to 4.2 times the integrated flux from the Permian plumes and four times of the integrated flux from the Four Corners plumes, two of the world's largest hotspots for oil and gas methane emissions. This work reveals the heavy-tailed distribution characteristic of CMM emission sources for the first time, with 20% of emitters contributing approximately 50% of total emissions. Comparison with the Global Energy Monitor (GEM) inventory reveals that the GEM estimate is about 4.1 times our estimate.

Plain Language Summary This study examines methane emissions from coal mines in Shanxi, China, identified as a significant source of global methane, a potent greenhouse gas. Using satellite data over 2 years, we found 138 detected episodic events at 82 facilities in Shanxi emitting an estimated 1.2 million tons of methane annually, far exceeding emissions from known global hotspots in the oil and gas sectors. Our analysis shows that a small percentage of these facilities contribute to the majority of emissions. The results, which challenge previous estimates from environmental monitoring organizations, underscore the need for direct, observational methods to accurately assess and address methane emissions. This work aims to guide efforts in mitigating climate change by identifying key areas for reducing methane release.

1. Introduction

Methane (CH_4) is responsible for around 30% of the rise in global temperatures since the Industrial Revolution, second only to carbon dioxide (Masson-Delmotte et al., 2021). The rapid increase in atmospheric methane concentrations in recent years is of concern (Lan et al., 2022), likely due to concurrent increases in emissions from fossil fuel extraction and microbial sources (Jackson et al., 2020; Peng et al., 2022; Thompson et al., 2018; Turner et al., 2019). Success in meeting the Paris Agreement and Global Methane Pledge depends greatly on the accessible, credible, and comparable Greenhouse Gas Inventory (GHGI). GHGIs reported by official public bodies, such as to the UN Framework Convention on Climate Change (UNFCCC), are typically constructed using bottom-up (BU) approaches in which activity data (e.g., number of facilities) are multiplied by emission factors (e.g., methane emitted per facility) (Buendia et al., 2019). However, significant discrepancies exist between these inventories and measurement-based estimates, both at the national and facility levels (Z. Chen et al., 2022; Irakulis-Loitxate et al., 2021; Lu et al., 2023; Sadavarte et al., 2021; Shen et al., 2022; Zhang et al., 2020). Advances in satellite monitoring technologies have enabled the quantification of individual methane emission

sources and attribution to specific facilities. Accurate accounting of methane emission with satellite measurements is of vital importance to verifing GHGI independently and globally, and facilitating targeted action, boosting our understanding of methane emissions (Jacob et al., 2022).

The latest report from the Intergovernmental Panel on Climate Change highlighted challenges and opportunities for mitigating methane (Core Writing Team & (eds.), 2023), with a special emphasis on reducing methane emissions from the fossil-fuel industry given their substantial contribution, cost-effectiveness and rapid response (Hmiel et al., 2020; Kemp & Ravikumar, 2021; Lin et al., 2019; Nisbet et al., 2020). Much of the previous research has focused on methane emissions from the oil and gas sector (Y. Chen et al., 2022; Duren et al., 2019; Ehret et al., 2022; Irakulis-Loitxate et al., 2021, 2022; Lauvaux et al., 2022; Lyon et al., 2016; Omara et al., 2022; Yu et al., 2022), with limited attention to coal mine methane (CMM). However, CMM may actually be a bigger contributor than oil or gas (Tate, 2022), with emissions set to grow considerably in the coming years (Kholod et al., 2020; Miller et al., 2019). CMM refers to methane emitted during coal extraction, which escapes from coal seams and is often siphoned off through ventilation systems to ensure a safe environment for miners.

China is the largest coal producer in the world (IEA, n.d.-a), with over 10,000 operating coal mines in 2011 (State Administration of Mine Safety (SACMS). Compilation of National Coal Mine Methane Level Identification for 2011, 2012) and about 5,000 operating coal mines in 2019 (National Energy Administration). Provincial coal mine production capacity announcement for 2019, n.d.). The IEA estimates that China's CMM emissions are 20.2 Mt in 2022, accounting for about half of the global CMM emissions (IEA, n.d.b). Shanxi is the province with the highest coal production and the largest number of coal mines in China. Its coal production is approximately equal to the combined output of the United States, Russia, and Australia. The CMM emissions in Shanxi are estimated to be between 5.8 and 13.1 Mt/yr (Liu et al., 2021; Peng et al., 2023; Scarpelli et al., 2022; Tate, 2022). Comprehensive CMM survey in Shanxi facilitates the specific emission factor (EF) updates and the opportunity to tackle these emissions.

In this work, we perform the first large-scale and high-resolution survey of CMM emitters over Shanxi, using spaceborne imaging spectrometer observations, supplemented by ground-based measurements for validation. We expose 82 anthropogenic methane emitters from space, captured by the Advanced Hyperspectral Imager (AHSI) onboard China's Gaofen-5B (GF5B), and identify different categories of these coal mines. And we apply the integrated methane enhancement (IME) method to estimate the emission rates. Lastly, We compare the satellite-derived methane emission rates with some bottom-up inventories.

2. Materials and Methods

2.1. Methane Inventories

In addition to some publicly available inventories like CEDS (O'Rourke et al., 2021) and EDGAR (Monforti Ferrario et al., 2021), we also collected basic information (including coal mine names and annual production) for 649 coal mines from the Shanxi Energy Bureau. Among them, 248 coal mines reported more detailed information including gas levels and mining depths. We obtained the locations of these 649 coal mines using the Baidu Maps API (https://lbsyun.baidu.com/) and represented them in the WGS coordinate system. It's worth noting that the State Administration of Coal Mine Safety provided information on China's coal mines in 2011, of which there were more thane 10,000 coal mines in China. Over the past decade, China's coal production grew by 60% while the number of coal mines decreased by 53%. This was mainly due to China's coal industry capacity reduction policy, which led to the closure of coal mines with low efficiency coal production. Therefore, bottom-up inventories of CMM emissions created based on this data should be used with caution.

The Global Coal Mine Tracker data set from Global Energy Monitor (GEM) provides information on the world's operating coal mines and their associated annual production capacity. This continuously updated data set integrates information from a wide range of sources, including government statistics, company reports, national and international NGO publications, and media reports. For this study, the data set (accessed in May 2022) was used to obtain key parameters for coal mines in Shanxi Province, including geospatial coordinates, production capacities, operation status, and owning companies. This allowed comprehensive characterization of the province's coal mining landscape to support the spatial attribution of detected methane enhancement signals.

2.2. Space-Based Observations

We use the hyperspectral data from the GaoFen-5B (GF5B) satellite operated by the China Center for Resources Satellite Data and Application (CCRSDA), which has almost the same sensor parameters as GF5. GF5B is equipped with the Advanced Hyperspectral Imager (AHSI) and has a local overpass time of ∼13:30. AHSI provides 330 spectral channels of feature spectral information with 60 km width, 30 m spatial resolution, and 400–2,500 nm spectral range (spectral resolution: 5–10 nm) since its launch in September 2021. We obtain a total of 165 images between October 2021 and February 2023 to cover Shanxi Province. We retrieve methane column enhancements quantitatively using methane absorption features in the shortwave infrared (SWIR) at 2,110–2,450 nm. The retrieval is limited by the heterogeneous or dark surfaces. Our identification of methane plumes in the enhancement maps is based on visual inspection.

2.3. Methane Retrievals

We perform the methane column enhancement (ΔXCH_4) retrieval with matched filter (MF) method, an approach often used by previous works on spaceborne detection. MF retrieve ΔXCH_4 by minimizing a cost function, the difference between observed and modeled spetrum. The methane column enhancements referred to here represent the difference between the methane column concentration (XCH_4) and the background. We model the background radiance as a multivariate Gaussian with mean μ and σ. These parameters are estimated on a per-column basis given the different radiative responses of the detector elements in different across-track. According to Beer Lambert's law, the spectrum affected by the methane concentration enhancement (x_m) can be modeled as,

$$x_m = x_b e^{-k\Delta c}. \tag{1}$$

Here x_r is the background spectrum, which is not affected by the methane concentration enhancement. Δc is the methane column enhancements and k is the unit methane absorption coefficient, which is extracted from simulated radiance by the MODTRAN model, following Pei et al. (2023). Then Δc can be retrieved by fitting the observed radiance spectrum (x) and modeled radiance spectrum (x_m) in the SWIR spectral region:

$$\Delta c = \frac{(x-\mu)^T \Sigma^{-1} \mu k}{k^T \Sigma^{-1} \mu k}. \tag{2}$$

We define a polygon to isolate the plume from the background based on visual inspection. We estimate methane emission rates (Q) in kilograms per hour (kg/h) based on the retrieved methane column enhancements in the last step. The Q is calculated using IME method, an approach often used by previous works. The IME method relates the total plume mass detected downwind of the source to the emission rate by

$$IME = \sum_{i=1}^{N} \Delta\Omega_i A_i, \tag{3}$$

where $\Delta\Omega_i$ and A_i are the methane column mass enhancement (kg/m^2) and area (m^2) of the ith pixel, respectively. N is the number of total pixels. Following Varon et al. (2018), we relate IME and Q as

$$Q = \frac{U_{eff} \cdot IME}{L} \tag{4}$$

where U_{eff} is the effective wind speed (m/s) and L is the square root of the masked plume area (m). The U_{eff} is derived from the measurable 10m wind speed U_{10} as

$$U_{eff} = 0.34 \cdot U_{10} + 0.44. \tag{5}$$

This empirical relationship between U_{eff} and U_{10} is estalished from a set of large eddy simulations (Irakulis-Loitxate et al., 2021). U10 data are taken from the GEOS-FP data set (Molod et al., 2012).

10.1029/2024GL109065

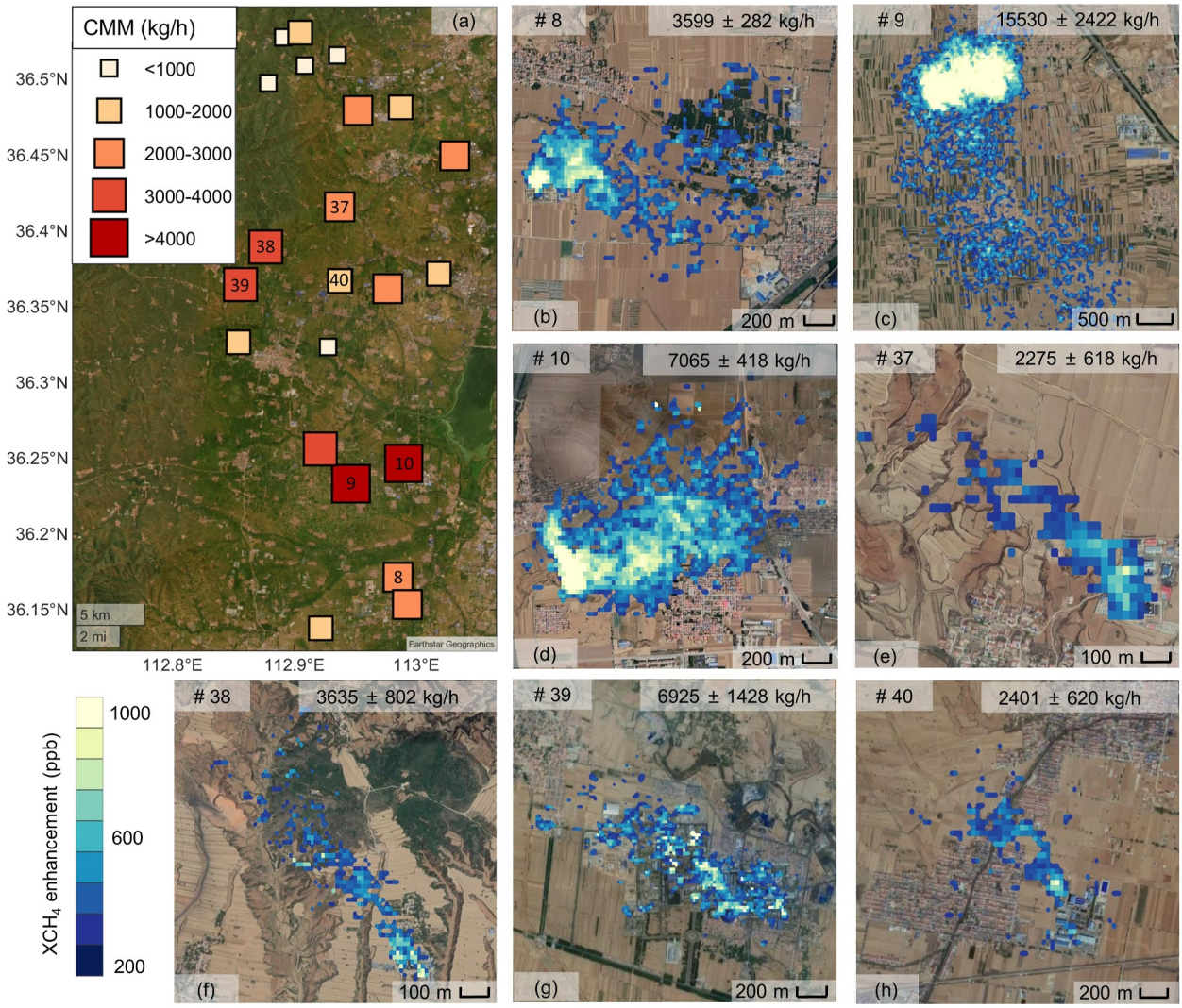

Figure 1. CMM point sources detected in Changzhi by GF5B. Emissions are size-coded and color-coded according to their emission rates in the main panel (a). Plume examples colored by methane column enhancements are shown in small panels (b–h). All of these emissions are associated with ventilation shafts, identified by satellite visible images and verified by ground crews.

3. Results

3.1. Spatial Pattern of Point Sources

Here we capitalize on 2 years of (from 2021.10 to 2023.02) cloud-free hyperspectral observations from GF5B to derive methane column enhancements at hyperfine resolution to identify and quantify the world's main CMM hotspot, down to the point sources. Figure S1 in Supporting Information S1 offers an overview of the study region, with 156 available GF5B images covering all coal mines in Shanxi province at least once over the 2-year period. We retrieved methane enhancement maps from the shortwave infrared spectra using the widely used matched filter algorithm. The hyperfine resolution of 30 m was sufficient to identify plumes and attribute them to ground facilities. Through careful examination of the methane enhancement maps, aided by visible satellite imagery and wind data, we identified a total of 138 individual methane plumes emanating from 82 distinct point sources over Shanxi. Figures S2–S4 in Supporting Information S1 provides definitive spectral evidence that methane is the primary contributor to the detected spectral differences. Several typical examples of methane plumes over Changzhi are shown in Figure 1.

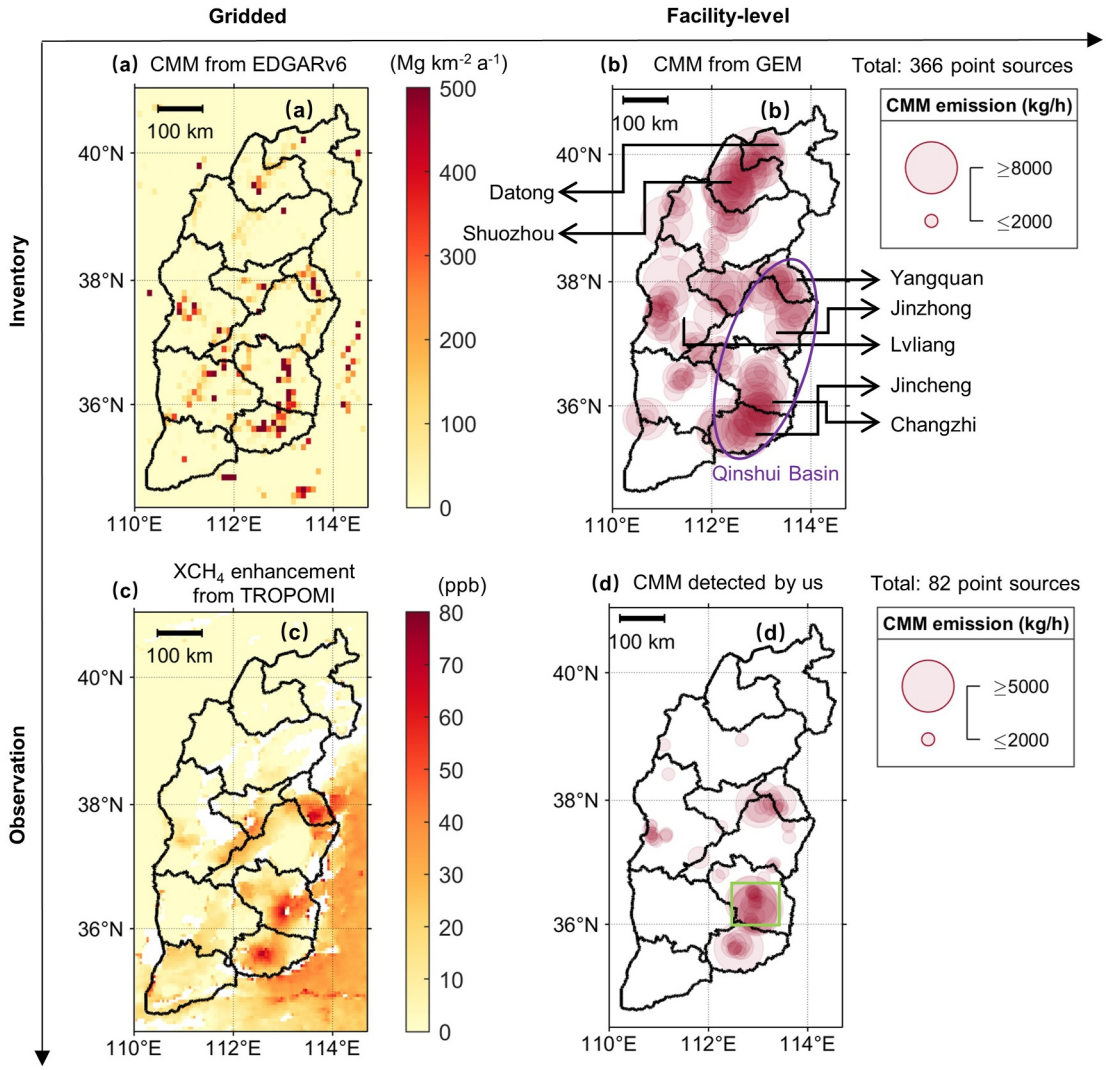

Figure 2. Inventories and satellite observations at grid level and facility level. (a) Bottom-up coal mine methane (CMM) inventory with 0.1 × 0.1° resolution from EDGARv6 (Monforti Ferrario et al., 2021). (b) Bottom-up CMM inventory from Global Energy Monitor. (c) Methane column enhancement with 5.5 × 7 km^2 pixel resolution derived from TROPOMI. (d) CMM emitters detected by GF5B in Shanxi. Cities in Shanxi are denoted in panel (b) with the purple ellipse showing roughly the Qinshui Basin.

The Qingshui basin (including cities of Changzhi, Jincheng and Yangquan) is considered to be the largest coalbed methane (CBM) production basin in China, accounting for 60% of China's total production in 2017 (Zhang et al., 2022). Our result reveals a high density of methane emitters over this area, which together respresent ~65% of the total detected point sources. Changzhi alone contains 34 (41%) point sources. Among them, 19 (56%) are found to be associated with coal mine vents. Establishing effective gas extraction and utilization systems is especially critical in China, where coal accounts for a major share of energy supply, in order to ensure safe operations, reduce environmental impacts, and harness energy resources. Several of these point sources have been detected by satellites in previous studies and their instantaneous emissions quantified using the PRISMA satellite (Guanter et al., 2021). To confirm these point sources, we conducted field measurements with the PICARRO equipment in Changzhi, and there were significant concentration peaks downwind of the detected point sources (see Figure S5 in Supporting Information S1). However, quantifying point source emissions using ground-based in-situ measurements remains challenging, thus we only performed qualitative analysis here.

Figure 2 illustrates inventory and satellite observations at the grid level and facility level. The XCH_4 observations are spatially consistent with the inventory, except for northern Shanxi (mainly Datong and Shuozhou). This indicates the inventory may be overestimated in this region, and our results further verify this view. Although the

bayesian-based flux inversion can adjust the prior fluxes based on the concentration observations and atmospheric transport model, the biased prior fluxes and wrong spatial distribution would pose great challenges for the inversion. In this work, despite limitations in directly observing the coal mines, we surmise that coal mines in the north emit far less methane than might be expected. It is worth noting that in Shanxi, 8 out of the 9 coal mines with annual production exceeding 10 million tonnes are located in northern Shanxi (Datong and Shuozhou). Figure S6 in Supporting Information S1 illustrates CMM extraction volume and utilization rate in China from 2005 to 2018. We speculate that the underestimation of CMM inventories in the north may be due to lack of consideration of CBM exploitation or underestimation of emission factors for the specific coalfield type. Methane emissions during the coal mining can be greatly reduced due to the "CBM extraction first, coal mining second" strategy (Zhang et al., 2022). This strategy not only increases energy supply (including both coal and coalbed methane) but also reduces methane emissions. To our knowledge, a large coal mine in the north has made major breakthroughs in gas extraction and purification technologies in recent years (Tao et al., 2019). Unlike CO_2 emission inventories, compilation of CMM inventories need to take account of not only coal production and emission factors, but also prior CBM extraction and CMM recovery rates.

3.2. Emission Intensity and Categorization of Point Sources

Distinguishing between highly intermittent and highly persistent point sources would be beneficial for determining emission factors, inferring annual emissions and potential mitigation actions. Owing to the 16-day revisit cycle and clouds effect, point sources were effectively sampled at most 10 times (average 4.6 times) during 2-year observation, showing 43% average persistance. This represents the frequency of plume detection ($f = M/N$), where M is the number of plumes detected at that source location and N is the number of overpasses over that location. Sufficient overpasses and low detection limit allowed for the persistence-weighted mean emission rate for each source using the methodology described in Cusworth et al. (2021). Table S1 in Supporting Information S1 shows mean emission rate for different persistent levels. We find that persistent sources ($f = 1$) constitute 13.4% of the total point sources, but are responsible for 32% of total emissions. These point sources are considered to be persistent leaks that require attention and emission curbs by the relevant authorities. Conversely, 33 (40%) highly intermittent sources ($f \leq 0.25$) accounted for 22% of the total emissions, which may be attributed to easily predictable emissions due to routine mining. Low-emission sources (0–500 kg/hr) accounted for 17% of all detected facilities and were highly intermittent (average $f = 0.26$). In contrast, detected sources above 4,000 kg/hr accounted for only 9% of the detected facilities but were more persistent (average $f = 0.89$).

Figures 3a and 3b and Figure S7 in Supporting Information S1 shows the distribution of persistence-adjusted emission rates from all the detected plumes in Shanxi Province. Overall, the emission rates of 138 individual plumes range from 474 to 19,290 kg/hr, which follow a lognormal distribution, a heavy-tail characteristic. The top 20% of sources contributed approximately 50% of the total emissions, with emission rates greater than 2,500 kg/hr. Previous works have reported heavy-tailed characteristics of the methane emission distribution from the oil and gas industry. To our knowledge, this work represents the first characterization of the CMM landscape through direct observations on a regional scale. However, we acknowledge satellite observations have greater detection limits compared to airborne imaging spectrometers. Our plume detection only represents instances when instantaneous emission rates exceeded detection limit at satellite overpass times. This implies that our persistence-adjusted emission rates are conservative estimates. The absence of an identifiable plume under cloud-free conditions may be due to emission rates below detection limits. Capturing intermittent nature and accurately inferring that annual emissions require frequent observations with lower detection limit (Cusworth et al., 2021; Frankenberg et al., 2016) or continuous ground-based observations (Qin et al., 2023).

Due to the variable meteorology and heterogeneous terrain, emission estimates from individual plumes can have high uncertainties, mainly from wind speed errors. However, the overestimations and underestimations of individuals caused by the variable conditions tend to cancel out in aggregate statistically. Most emissions are intermittent, and we assume individual snapshots are randomly distributed in time. This means our long time-series and large-scale observations provide statistical samples of the regional large emitters, enabling representative annual regional emission estimates, albeit with significant uncertainty (Frankenberg et al., 2016; Irakulis-Loitxate et al., 2021). Summing up all emissions yields a regional total of ~1.20 Mt/yr, explaining about 16% of the previously reported total of 7.74 Mt/yr (Scarpelli & Jacob, 2019). The warming effect of 1.2 Mt of methane emissions is equivalent to 98.4 Mt of carbon dioxide, which is roughly equivalent to Czechia's national CO_2 emissions (101.54 Mt) in 2022. Although we can only probe extreme point sources, we still surmise the

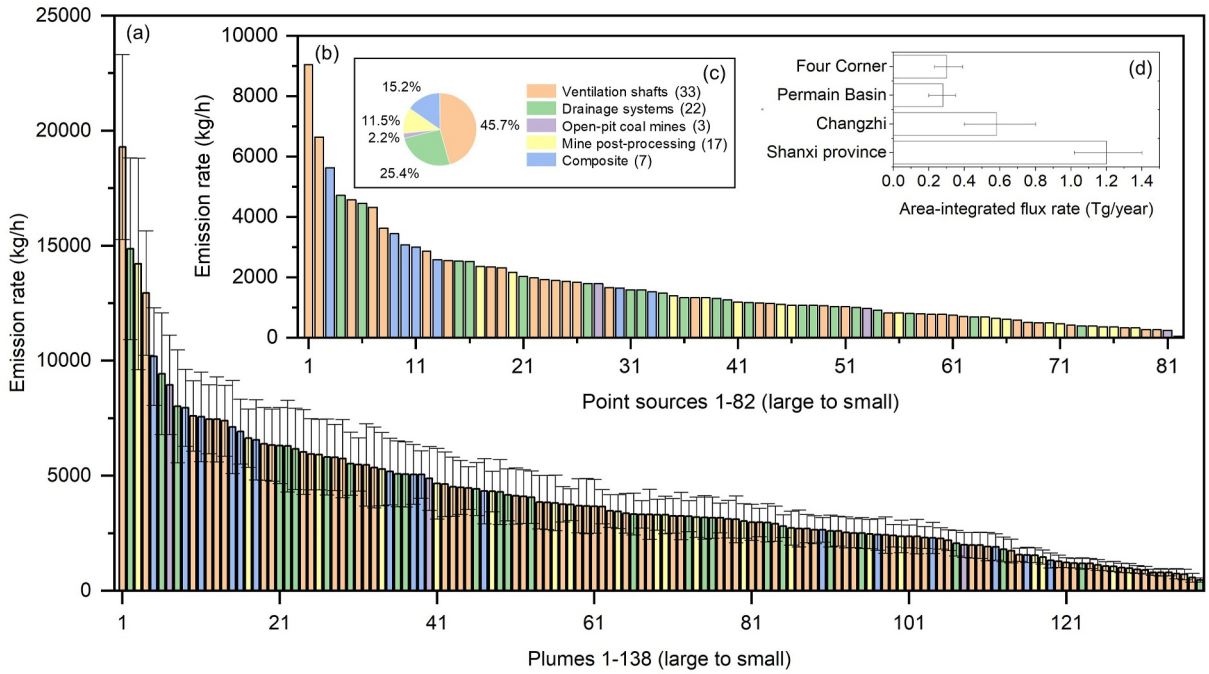

Figure 3. Distribution of emission rates for the 138 plumes (a) and the corresponding 82 point sources (b) detected in Shanxi Province. (c) Categorization of 82 emission point sources detected in Shanxi Province. The numbers next to the pie chart indicate the percentage of total emissions detected in each category. (d) Comparison of regional flux estimates detected over Shanxi and Changzhi by the GF5B-AHSI, over the Four Corners region by AVIRIS-NG, and over the Permain Basin by GF5-AHSI. Error bars correspond to the 95% confidence interval in regional flux estimates.

bottom-up inventories may be overestimated for this region, according to the almost non-detection of emitters in northern Shanxi mentioned previously, as well as the comparison with facility-level inventories in the next section. Given the retrieval complexity and intermittent of point sources, the uncertainty of regional total flux obtained from complete theoretical error propagation may not be meaningful. Instead, we carried out a nonparametric bootstrap analysis, following Frankenberg et al. (2016). This yielded a 95% confidence interval of 0.98 Mt/yr to 1.44 Mt/yr for the total regional emissions in Shanxi. Figure 3d compares the total emissions from the extreme point sources in Shanxi, Changzhi, Permian Basin (Irakulis-Loitxate et al., 2021), and Four Corner region (Frankenberg et al., 2016), which are 1.2, 0.58, 0.28, and 0.3 Mt/yr respectively. The integrated flux from Shanxi plumes is roughly 4.2 times that of the Permian Basin and four times that of the Four Corners region. Here integrated flux from plumes refer to the total emissions from the detected plumes rather than the total emissions over the corresponding area. The annual emission from Four Corner region, with an area of about 3,200 km^2, is 0.3 Mt/yr (0.23–0.39 Mt/yr 95% confidence interval) (Frankenberg et al., 2016), whereas the annual emission from Changzhi, with an area of about 14,000 km^2, is 0.58 (0.40–0.80 Mt/yr 95% confidence interval) Mt/yr. The aforementioned results are derived using persistence-adjusted emission rates. However, locally calm winds or heterogeneous dark terrain can lead to higher lower detection limits, meaning that small emission point sources can no longer be detected. Neglecting plume detection frequencies and extrapolating aggregated emission distributions yields a 2.85 (+0.38/−0.35) Mt/yr estimate for total regional emissions.

According to field surveys and Google Earth imagery analysis, we categorized ground facilities into five types: ventilation shafts, drainage systems, open-pit coal mines, mine post-processing, and composite. Ventilation shafts refer to methane extracted from underground coal mines that is directly released into the atmosphere to mitigate mining hazards. The drainage system pumps gas from the coal seam or mining area to the surface for reuse by drilling, using boreholes, pipes and vacuum pumps. However, some fraction of methane may leaks into the atmosphere due to equipment issues or unstable concentration of extracted methane. The key difference from drainage systems is that no pipelines or gas tanks are visible around ventilation shafts, suggesting no intention of CMM recovery. Figure 3c shows the categorization results for the 82 point sources. Our results indicate that ventilation shafts contribute overwhelmingly to total emissions and source numbers, with the top 1 emission source being ventilation shafts. The three open-pit coal mines and 17 mine post-processing facilities account for

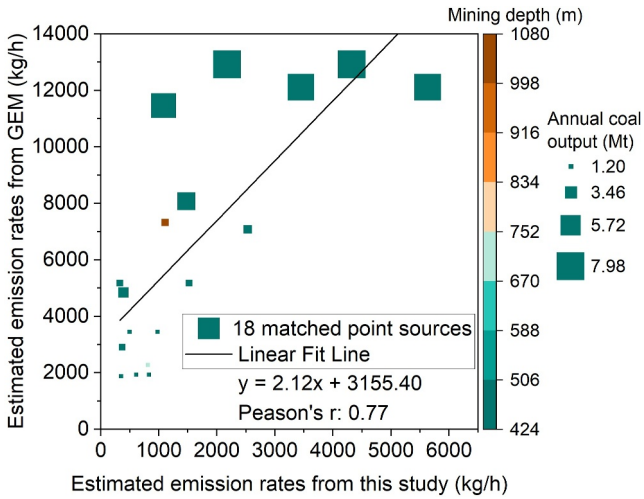

Figure 4. Estimated emission rates from this study (*x* axis) against GEM's estimates (*y* axis). Scatters are size-coded and color-coded by their mining depth and annual coal output, respectively. The black line is a linear regression of the data, with the equation of this best-fit line shown on the plot.

2.2% and 11.5% of total emissions, respectively. Additionally, there are seven emission sources that are composite facilities, including gas extraction and mine post-processing. Notably, point source #52 was overpassed twice over 2 years, with a detection frequency of 0.5. After confirmation by the ground crew, this source is a natural gas transport-related plant area and categorized as mine post-processing, typical of intermittent emission sources. Figure S8 in Supporting Information S1 shows the Google Earth imagery for this location, with numerous gas tanker trucks gathered.

3.3. Comparisons With Bottom-Up Inventories

Figure S9 in Supporting Information S1 compares our emission estimates with previous bottom-up inventories. While largely consistent in temporal trends, significant discrepancies exist across different bottom-up inventories, differing by up to 4.3 Mt/yr in 2020 estimates for Shanxi. Since our findings only represent extreme point emitters in the province, comparing single site emissions to gridded flux maps is only illustrative of spatial distributions, further emphasizing the magnitude of our observed point source sums. Overall, the spatial patterns of CMM discussed above are consistent with bottom-up inventories based on production data and emission factor in most regions. These bottom-up inventories give Shanxi province emissions estimates of 6.2–10.5 Mt/yr for 2,020, 5.1 to 8.8 times our summed estimate from the 82 point sources detected.

For a mine-level comparison, we have also compared our detected emissions against the bottom-up inventory provided GEM (see Section 2). Of these 82 detected sources, only 18 sources passes the position match test (less than 600 m). This suggests that the coal mine locations provided by GEM may differ from the actual release locations. Figure 4 demonstrates the comparison results of these 18 coal mines, which exhibits high correlation with an R of 0.77. GEM estimates are on average 4.1 times our observed emissions, suggesting potential overestimation in other bottom-up approaches. In addition to determining emission factors specific to coal field types and mining depth, future CMM inventory compilation should account for pre-mining CBM utilization as well as CMM recycling. Additionally, we scraped the locations of 689 coal mines in Shanxi using the Baidu Maps API based on mine names from the Shanxi Energy Bureau. However, the detected source locations differed substantially from the API-derived points, which mark coal company offices far from actual ventilation shafts. This highlights that future inventory compilation cannot solely rely on company office coordinates from maps.

4. Conclusions and Discussion

Our satellite-based approach has enabled the first provincial-scale survey of CMM point sources across Shanxi, China's top coal-producing region. The 30-m resolution GF5B imaging spectrometer used in this study has proven to be effective for detecting, quantifying and attributing strong methane plumes to their facility origins. We identified 82 major emitters using matched filter method, largely clustered in the southeast Changzhi city. Employing the IME method to estimate emission rates, our findings reveal emission intensities ranging from 474 to 19,290 kg/hr, highlighting the heavy-tail distribution of CMM emissions in Shanxi Province. The top 20% of sources contributed approximately 50% of the total emissions, with emission rates greater than 2,500 kg/hr.

Our results underscore the significant discrepancies between existing bottom-up Greenhouse Gas Inventories (GHGIs) and measurement-based estimates, especially in coal mining areas in northern Shanxi. It is important to note that the total emissions reported in this work refer to the integrated flux from plumes, distinct from total emissions reported in bottom-up inventories and top-down inversions. This is the primary reason for the substantial differences between our total emissions and those reported previously. Mine-level comparison with the GEM inventory preliminarily reveals that there is an overestimation of the inventory by a factor of about 4.1. Previous top-down studies typically reveal that emissions inventories are underestimated in most regions (Kort et al., 2014; Sadavarte et al., 2021; Wei et al., 2023). However, in the Shanxi region, our findings contradict this trend. Recent top-down inversion studies also suggests overestimation in the inventory for the Shanxi region (Shen et al., 2023; Zhang et al., 2022). We suggest that the overestimation of bottom-up inventories is associated

with extraction of CBM. The strategy of "extracting CBM before coal mining" may lead to sizable reduction in methane emissions during the coalmining phase.

The findings emphasize the critical value of satellite observations for independently verifying and globally monitoring GHGI, offering crucial data for the quantification and attribution of CMM emissions, thereby supporting targeted mitigation measures. Significantly, this study delineates the intermittent characteristics of methane emissions across various facility types and highlights the critical role of ventilation shafts. These shafts not only predominate in terms of the emitter count but also in their contribution to the aggregate emissions. This insight underscores the importance of persistence factors in determining emission factors, inferring annual emissions, and identifying potential mitigation actions.

However, attention must be given to the uncertainties associated with retrieved concentration enhancements, which are influenced by limitations in spectral resolution and signal-to-noise ratio. Additionally, the heterogeneous surface of Shanxi results in a higher detection limit, posing significant challenges to the automated extraction of plumes. Consequently, many point sources with low emission rates may remain undetected and unquantified, leading to conservative estimates of the total emissions.

Going forward, In addition to the operational GF5B, PRISMA, EnMAP and EMIT satellites, upcoming high-resolution imaging spectrometers such as CHIME, Carbon Mapper and MethaneSAT will further improve the revisit frequency of methane point source characterization globally. In tandem with densified in-situ monitoring networks, these observations promise for information for Methane Alert and Response System (MARS) (Guanter et al., 2023), robust methane inventory compilation and mitigation policy assessments.

Data Availability Statement

The gridded inventories are available from CEDS (O'Rourke et al., 2021) and EDGAR (Monforti Ferrario et al., 2021). The Global Coal Mine Tracker data set is obtained from GEM, available at https://globalenergymonitor.org/projects/global-coal-mine-tracker/. The U_{10} data is obtained from GEOS-FP data set, available at https://portal.nccs.nasa.gov/datashare/gmao/geos-fp/das/. The GF5B methane column enhancement data that support the findings of this study are publicly available Pei (2024). All codes are available at https://github.com/peisipand/GF5_MF_CH4.

Acknowledgments
The study was supported by the National key research and development program (Grant 2022YFB3904801) and National Natural Science Foundation of China (Grant 4197283, 41827801). The authors would like to thank the China Centre For Resources Satellite Data and Application for the free GF5B data used in this study. This research is supported in part through computational resources provided by the Supercomputing Center of Wuhan University.

References

Buendia, C. E., Tanabe, K., Kranjc, A., Baasansuren, J., Fukuda, M., Ngarize, S., et al. (2019). *2019 refinement to the 2006 IPCC guidelines for national greenhouse gas inventories*. IPCC. Retrieved from https://www.ipcc.ch/report/2019-refinement-to-the-2006-ipcc-guidelines-for-national-greenhouse-gas-inventories/

Chen, Y., Sherwin, E. D., Berman, E. S., Jones, B. B., Gordon, M. P., Wetherley, E. B., et al. (2022). Quantifying regional methane emissions in the New Mexico Permian basin with a comprehensive aerial survey. *Environmental Science & Technology*, *56*(7), 4317–4323. https://doi.org/10.1021/acs.est.1c06458

Chen, Z., Jacob, D. J., Nesser, H., Sulprizio, M. P., Lorente, A., Varon, D. J., et al. (2022). Methane emissions from China: A high-resolution inversion of Tropomi satellite observations. *Atmospheric Chemistry and Physics*, *22*(16), 10809–10826. https://doi.org/10.5194/acp-22-10809-2022

Core Writing Team & (eds.). (2023). Summary for policymakers. In *Climate change 2023: Synthesis report* (pp. 1–34). IPCC. https://doi.org/10.59327/IPCC/AR6-9789291691647.001

Cusworth, D. H., Duren, R. M., Thorpe, A. K., Olson-Duvall, W., Heckler, J., Chapman, J. W., et al. (2021). Intermittency of large methane emitters in the Permian basin. *Environmental Science and Technology Letters*, *8*(7), 567–573. https://doi.org/10.1021/acs.estlett.1c00173

Duren, R. M., Thorpe, A. K., Foster, K. T., Rafiq, T., Hopkins, F. M., Yadav, V., et al. (2019). California's methane super-emitters. *Nature*, *575*(7781), 180–184. https://doi.org/10.1038/s41586-019-1720-3

Ehret, T., De Truchis, A., Mazzolini, M., Morel, J.-M., D'aspremont, A., Lauvaux, T., et al. (2022). Global tracking and quantification of oil and gas methane emissions from recurrent sentinel-2 imagery. *Environmental Science & Technology*, *56*(14), 10517–10529. https://doi.org/10.1021/acs.est.1c08575

Frankenberg, C., Thorpe, A. K., Thompson, D. R., Hulley, G., Kort, E. A., Vance, N., et al. (2016). Airborne methane remote measurements reveal heavy-tail flux distribution in four corners region. *Proceedings of the National Academy of Sciences*, *113*(35), 9734–9739. https://doi.org/10.1073/pnas.1605617113

Guanter, L., Irakulis-Loitxate, I., Gorroño, J., Sánchez-García, E., Cusworth, D. H., Varon, D. J., et al. (2021). Mapping methane point emissions with the PRISMA spaceborne imaging spectrometer. *Remote Sensing of Environment*, *265*, 112671. https://doi.org/10.1016/j.rse.2021.112671

Guanter, L., Irakulis-Loitxate, I., Maasakkers, J. D., Aben, I., Lelong, C., Randles, C. A., et al. (2023). Methane alert and response system (Mars): IMEO's satellite-based system for detection and attribution of methane point sources around the world (Tech. Rep.). *Copernicus Meetings*.

Hmiel, B., Petrenko, V., Dyonisius, M., Buizert, C., Smith, A., Place, P., et al. (2020). Preindustrial 14ch4 indicates greater anthropogenic fossil ch4 emissions. *Nature*, *578*(7795), 409–412. https://doi.org/10.1038/s41586-020-1991-8

IEA. (n.d.a). *Coal 2022*. IEA. Retrieved from https://www.iea.org/reports/coal-2022,License:CCBY4.0

IEA. (n.d.b). *Global methane tracker 2023*. IEA. Retrieved from https://www.iea.org/reports/global-methane-tracker-2023,License:CCBY4.0

Irakulis-Loitxate, I., Guanter, L., Liu, Y.-N., Varon, D. J., Maasakkers, J. D., Zhang, Y., et al. (2021). Satellite-based survey of extreme methane emissions in the Permian basin. *Science Advances*, *7*(27), eabf4507. https://doi.org/10.1126/sciadv.abf4507

Irakulis-Loitxate, I., Guanter, L., Maasakkers, J. D., Zavala-Araiza, D., & Aben, I. (2022). Satellites detect abatable super-emissions in one of the world's largest methane hotspot regions. *Environmental Science & Technology*, *56*(4), 2143–2152. https://doi.org/10.1021/acs.est.1c04873

Jackson, R. B., Saunois, M., Bousquet, P., Canadell, J. G., Poulter, B., Stavert, A. R., et al. (2020). Increasing anthropogenic methane emissions arise equally from agricultural and fossil fuel sources. *Environmental Research Letters*, *15*(7), 071002. https://doi.org/10.1088/1748-9326/ab9ed2

Jacob, D. J., Varon, D. J., Cusworth, D. H., Dennison, P. E., Frankenberg, C., Gautam, R., et al. (2022). Quantifying methane emissions from the global scale down to point sources using satellite observations of atmospheric methane. *Atmospheric Chemistry and Physics*, *22*(14), 9617–9646. https://doi.org/10.5194/acp-22-9617-2022

Kemp, C. E., & Ravikumar, A. P. (2021). New technologies can cost effectively reduce oil and gas methane emissions, but policies will require careful design to establish mitigation equivalence. *Environmental Science & Technology*, *55*(13), 9140–9149. https://doi.org/10.1021/acs.est.1c03071

Kholod, N., Evans, M., Pilcher, R. C., Roshchanka, V., Ruiz, F., Coté, M., & Collings, R. (2020). Global methane emissions from coal mining to continue growing even with declining coal production. *Journal of Cleaner Production*, *256*, 120489. https://doi.org/10.1016/j.jclepro.2020.120489

Kort, E. A., Frankenberg, C., Costigan, K. R., Lindenmaier, R., Dubey, M. K., & Wunch, D. (2014). Four corners: The largest us methane anomaly viewed from space. *Geophysical Research Letters*, *41*(19), 6898–6903. https://doi.org/10.1002/2014gl061503

Lan, X., Thoning, K., & Dlugokencky, E. (2022). Trends in globally-averaged CH_4, N_2O, and SF6 determined from NOAA global monitoring laboratory measurements. https://doi.org/10.15138/P8XG-AA10

Lauvaux, T., Giron, C., Mazzolini, M., d'Aspremont, A., Duren, R., Cusworth, D., et al. (2022). Global assessment of oil and gas methane ultra-emitters. *Science*, *375*(6580), 557–561. https://doi.org/10.1126/science.abj4351

Lin, J., Khanna, N., Liu, X., Teng, F., & Wang, X. (2019). China's non-CO_2 greenhouse gas emissions: Future trajectories and mitigation options and potential. *Scientific Reports*, *9*(1), 16095. https://doi.org/10.1038/s41598-019-52653-0

Liu, G., Peng, S., Lin, X., Ciais, P., Li, X., Xi, Y., et al. (2021). Recent slowdown of anthropogenic methane emissions in China driven by stabilized coal production. *Environmental Science and Technology Letters*, *8*(9), 739–746. https://doi.org/10.1021/acs.estlett.1c00463

Lu, X., Jacob, D. J., Zhang, Y., Shen, L., Sulprizio, M. P., Maasakkers, J. D., et al. (2023). Observation-derived 2010-2019 trends in methane emissions and intensities from us oil and gas fields tied to activity metrics. *Proceedings of the National Academy of Sciences*, *120*(17), e2217900120. https://doi.org/10.1073/pnas.2217900120

Lyon, D. R., Alvarez, R. A., Zavala-Araiza, D., Brandt, A. R., Jackson, R. B., & Hamburg, S. P. (2016). Aerial surveys of elevated hydrocarbon emissions from oil and gas production sites. *Environmental Science & Technology*, *50*(9), 4877–4886. https://doi.org/10.1021/acs.est.6b00705

Masson-Delmotte, V., Zhai, P., Pirani, A., Connors, S. L., Péan, C., Berger, S., et al. (2021). Climate change 2021: The physical science basis. Contribution of working group I to the sixth assessment report of the intergovernmental panel on climate change, 2.

Miller, S. M., Michalak, A. M., Detmers, R. G., Hasekamp, O. P., Bruhwiler, L. M., & Schwietzke, S. (2019). China's coal mine methane regulations have not curbed growing emissions. *Nature Communications*, *10*(1), 303. https://doi.org/10.1038/s41467-018-07891-7

Molod, A., Takacs, L., Suarez, M., Bacmeister, J., Song, I.-S., & Eichmann, A. (2012). The GEOS-5 atmospheric general circulation model: Mean climate and development from MERRA to Fortuna. *Technical Reports Series*.

Monforti Ferrario, F., Crippa, M., Guizzardi, D., Muntean, M., Schaaf, E., Lo Vullo, E., et al. (2021). *Edgar v6.0 greenhouse gas emissions*. IEA. License: CC BY 4.0. Retrieved from https://www.iea.org/reports/global-methane-tracker-2023

National Energy Administration. (n.d.). Provincial coal mine production capacity announcement for 2019 (in Chinese). http://www.nea.gov.cn/ztzl/mtscnlgg/scnlgg.htm

Nisbet, E., Fisher, R., Lowry, D., France, J., Allen, G., Bakkaloglu, S., et al. (2020). Methane mitigation: Methods to reduce emissions, on the path to the Paris agreement. *Reviews of Geophysics*, *58*(1), e2019RG000675. https://doi.org/10.1029/2019rg000675

Omara, M., Zavala-Araiza, D., Lyon, D. R., Hmiel, B., Roberts, K. A., & Hamburg, S. P. (2022). Methane emissions from us low production oil and natural gas well sites. *Nature Communications*, *13*(1), 2085. https://doi.org/10.1038/s41467-022-29709-3

O'Rourke, P., Smith, S., Mott, A., Ahsan, H., Mcduffie, E., Crippa, M., et al. (2021). *Ceds v_2021_04_21 gridded emissions data*. PNNL DataHub. https://doi.org/10.25584/PNNLDataHub/1779095

Pei, Z. (2024). Replication data for: Unveiling unprecedented methane hotspots in China's leading coal production hub: A satellite mapping revelation [Dataset]. https://doi.org/10.5061/dryad.ncjsxksx2

Pei, Z., Han, G., Mao, H., Chen, C., Shi, T., Yang, K., et al. (2023). Improving quantification of methane point source emissions from imaging spectroscopy. *Remote Sensing of Environment*, *295*, 113652. https://doi.org/10.1016/j.rse.2023.113652

Peng, S., Giron, C., Liu, G., d'Aspremont, A., Benoit, A., Lauvaux, T., et al. (2023). High-resolution assessment of coal mining methane emissions by satellite in Shanxi, China. *iScience*, *26*(12), 108375. https://doi.org/10.1016/j.isci.2023.108375

Peng, S., Lin, X., Thompson, R. L., Xi, Y., Liu, G., Hauglustaine, D., et al. (2022). Wetland emission and atmospheric sink changes explain methane growth in 2020. *Nature*, *612*(7940), 477–482. https://doi.org/10.1038/s41586-022-05447-w

Qin, K., Hu, W., He, Q., Lu, F., & Cohen, J. B. (2023). Individual coal mine methane emissions constrained by eddy-covariance measurements: Low bias and missing sources. *EGUsphere*, *2023*, 1–49.

Sadavarte, P., Pandey, S., Maasakkers, J. D., Lorente, A., Borsdorff, T., Denier van der Gon, H., et al. (2021). Methane emissions from super-emitting coal mines in Australia quantified using tropomi satellite observations. *Environmental Science & Technology*, *55*(24), 16573–16580. https://doi.org/10.1021/acs.est.1c03976

Scarpelli, T. R., & Jacob, D. J. (2019). Global Fuel Exploitation Inventory (GFEI). *Harvard Dataverse*. https://doi.org/10.7910/DVN/HH4EUM

Scarpelli, T. R., Jacob, D. J., Grossman, S., Lu, X., Qu, Z., Sulprizio, M. P., et al. (2022). Updated global fuel exploitation inventory (GFEI) for methane emissions from the oil, gas, and coal sectors: Evaluation with inversions of atmospheric methane observations. *Atmospheric Chemistry and Physics*, *22*(5), 3235–3249. https://doi.org/10.5194/acp-22-3235-2022

Shen, L., Gautam, R., Omara, M., Zavala-Araiza, D., Maasakkers, J. D., Scarpelli, T. R., et al. (2022). Satellite quantification of oil and natural gas methane emissions in the US and Canada including contributions from individual basins. *Atmospheric Chemistry and Physics*, *22*(17), 11203–11215. https://doi.org/10.5194/acp-22-11203-2022

Shen, L., Jacob, D. J., Gautam, R., Omara, M., Scarpelli, T. R., Lorente, A., et al. (2023). National quantifications of methane emissions from fuel exploitation using high resolution inversions of satellite observations. *Nature Communications*, *14*(1), 4948. https://doi.org/10.1038/s41467-023-40671-6

State Administration of Mine Safety (SACMS). (2012). Compilation of national coal mine methane level identification for 2011 (in Chinese).

Tao, S., Chen, S., & Pan, Z. (2019). Current status, challenges, and policy suggestions for coalbed methane industry development in China: A review. *Energy Science & Engineering*, *7*(4), 1059–1074. https://doi.org/10.1002/ese3.358

Tate, R. D. (2022). Bigger than oil or gas?

Thompson, R. L., Nisbet, E., Pisso, I., Stohl, A., Blake, D., Dlugokencky, E., et al. (2018). Variability in atmospheric methane from fossil fuel and microbial sources over the last three decades. *Geophysical Research Letters*, *45*(20), 11–499. https://doi.org/10.1029/2018gl078127

Turner, A. J., Frankenberg, C., & Kort, E. A. (2019). Interpreting contemporary trends in atmospheric methane. *Proceedings of the National Academy of Sciences*, *116*(8), 2805–2813. https://doi.org/10.1073/pnas.1814297116

Varon, D. J., Jacob, D. J., McKeever, J., Jervis, D., Durak, B. O., Xia, Y., & Huang, Y. (2018). Quantifying methane point sources from fine-scale satellite observations of atmospheric methane plumes. *Atmospheric Measurement Techniques*, *11*(10), 5673–5686. https://doi.org/10.5194/amt-11-5673-2018

Wei, C., Jafari Raad, S. M., & Hassanzadeh, H. (2023). Estimation of natural methane emissions from the largest oil sand deposits on earth. *PNAS nexus*, *2*(9), pgad260. https://doi.org/10.1093/pnasnexus/pgad260

Yu, J., Hmiel, B., Lyon, D. R., Warren, J., Cusworth, D. H., Duren, R. M., et al. (2022). Methane emissions from natural gas gathering pipelines in the permian basin. *Environmental Science and Technology Letters*, *9*(11), 969–974. https://doi.org/10.1021/acs.estlett.2c00380

Zhang, Y., Fang, S., Chen, J., Lin, Y., Chen, Y., Liang, R., et al. (2022). Observed changes in China's methane emissions linked to policy drivers. *Proceedings of the National Academy of Sciences*, *119*(41), e2202742119. https://doi.org/10.1073/pnas.2202742119

Zhang, Y., Gautam, R., Pandey, S., Omara, M., Maasakkers, J. D., Sadavarte, P., et al. (2020). Quantifying methane emissions from the largest oil-producing basin in the United States from space. *Science Advances*, *6*(17), eaaz5120. https://doi.org/10.1126/sciadv.aaz5120